Opto-Electronic Advances

Original Article

2018, Vol. 1, No. 7

DOI: 10.29026/oea.2018.180012

An accurate design of graphene oxide ultrathin flat lens based on Rayleigh-Sommerfeld theory

Guiyuan Cao, Xiaosong Gan, Han Lin and Baohua Jia*

Graphene oxide (GO) ultrathin flat lenses have provided a new and viable solution to achieve high resolution, high efficiency, ultra-light weight, integratable and flexible optical systems. Current GO lenses are designed based on the Fresnel diffraction model, which uses a paraxial approximation for low numerical aperture (NA) focusing process. Herein we develop a lens design method based on the Rayleigh-Sommerfeld (RS) diffraction theory that is able to unambiguously determine the radii of each ring without the optimization process for the first time. More importantly, the RS design method is able to accurately design GO lenses with arbitrary NA and focal length. Our design is experimentally confirmed by fabricating high NA GO lenses with both short and long focal lengths. Compared with the conventional Fresnel design methods, the differences in ring positions and the resulted focal length are up to 13.9% and 9.1%, respectively. Our method can be further applied to design high performance flat lenses of arbitrary materials given the NA and focal length requirements, including metasurfaces or other two-dimensional materials.

Keywords: ultrathin flat lens; graphene oxide; Rayleigh-Sommerfeld diffraction; Fresnel diffraction

Cao G Y, Gan X S, Lin H, Jia B H. An accurate design of graphene oxide ultrathin flat lens based on Rayleigh-Sommerfeld theory. *Opto-Electronic Advances* **1**, 180012 (2018).

Introduction

Flat lenses made of ultrathin materials have the advantages of astigmatism and coma aberrations free, which are otherwise common problems for conventional curved surface lenses, especially when the numerical aperture (NA) is high[1]. In addition, flat lenses offer a compact design for a myriad of rapid development of nanophotonics and integrated photonic systems, as well as electro-optical applications, such as solar cells and fiber communication systems. A number of ultrathin flat lens concepts[2–6] have been proposed, such as metamaterials[7], metasurfaces[8] and planar diffraction lenses[9–11]. Recently, planar diffraction lenses have attracted much attention due to the possibility to achieve wide operational bandwidth[12], chromatic aberration compensation[13] and high focusing performance. Among them, graphene oxide (GO) ultrathin flat lenses[11,14,15] have demonstrated attractive properties, such as nanometer thickness, high focusing resolution and efficiency, high mechanical strength and flexibility, and fast and low-cost fabrication process. In addition, the GO ultrathin flat lens can potentially be integrated onto various optical components to change or optimize their functionalities, such as conventional optical lenses, fiber tips, and on chip optical systems.

The current GO lenses are designed using the Fresnel diffraction model[16–21], which is only applicable for lenses with a low NA satisfying the paraxial approximation. For a high NA lens, it is not able to accurately predict the focusing performance. While the vigorous finite difference time domain (FDTD) method[8,22–24] provides accurate simulation on the focusing process, the required amount of computational memory and time increase significantly as geometry progression. One simulation could take days. As a result, the FDTD method is limited to lenses with a focal length less than 10 μm. Therefore, to promote practical GO lens applications, it is necessary to develop a theoretical modeling method that is able to accurately calculate the focusing process of GO lenses with arbitrary NA and focal lengths with high speed and efficiency and low computational cost. Such a model can be equally applicable to other ultrathin lens with high NA and large focal length.

In this paper, we develop an accurate method based on

Centre for Micro-Photonics, Faculty of Engineering, Science and Technology, Swinburne University of Technology, John Street, Hawthorn, VIC 3122, Australia

* Correspondence: B H Jia, E-mail: bjia@swin.edu.au

Received 1 July 2018; accepted 26 July 2018; accepted article preview online 21 August 2018

the Rayleigh-Sommerfeld (RS) diffraction theory without the paraxial constrain to design GO ultrathin flat lens. The ring radii of a desired GO lens is decided directly from the RS diffraction theory without the optimization process, such as iterative[25], local optimization algorithm[26] and global-search-optimization algorithm[27], that is normally used in other design methods for high NA lenses. Most importantly, the RS design method is able to design GO lenses with arbitrary NA, size and focal length. To verify our RS design method, we designed two GO lenses with focal lengths of 3.1 μm (*NA*=0.82) and 9.1 μm (*NA*=0.71), respectively. The designs were verified both theoretically by FDTD simulation and experimentally by laser fabrication and point spread function characterization.

Theoretical model

The schematic of the GO lens focusing is shown in Fig. 1(a). The incident light wave ($U_1(r_1,\theta_1)$) is propagating along the positive z direction. The amplitude and phase of the incident light that are modulated by the GO lens become $U_1'(r_1,\theta_1)$. The GO lens plane is the diffraction plane, $r_1=(x_1^2+y_1^2)^{1/2}$, r_1 and θ_1 are the polar coordinates in the GO lens plane. The $r_2-\theta_2$ plane is the observation plane, which is usually the focal plane. $r_2=(x_2^2+y_2^2)^{1/2}$, r_2 and θ_2 are the polar coordinates in the focal plane. z is the distance between the diffraction plane and the observation plane.

According to the RS diffraction theory[28–30], the field at an arbitrary observation plane at a distance z can be written as:

$$U_2(r_2,\theta_2,z)=\frac{1}{2\pi}\int_0^{2\pi}\int_0^{\infty}U_1'(r_1,\theta_1)(-\mathrm{i}k-\frac{1}{\sqrt{\varepsilon}})\cdot\frac{\exp(-\mathrm{i}k\sqrt{\varepsilon})}{\varepsilon}zr_1\mathrm{d}r_1\mathrm{d}\theta_1\ ,\qquad(1)$$

$$\varepsilon=z^2+r_1^2+r_2^2-2r_1r_2\cos(\theta_1-\theta_2)\,,$$

where $k=2\pi/\lambda$ is the wave vector, λ is the wavelength of the incident beam in vacuum; $U_1'(r_1,\theta_1)$ is the E-field immediately behind the GO ultrathin flat lens. When the incident wave $U_1(r_1,\theta_1)$ impinges on the GO lens, the beam is partly absorbed and diffracted by the reduced graphene oxide (rGO) and GO zones. $U_1'(r_1,\theta_1)$ can be expressed as[28]:

$$U_1'(r_1,\theta_1)=U_1(r_1,\theta_1)\,t(r_1,\theta_1)\exp[-\mathrm{i}k\cdot\Phi(r_1,\theta_1)]\,,\qquad(2)$$

where $t(r_1,\theta_1)$ is the transmission coefficient, $\Phi(r_1,\theta_1)$ is the phase modulation provided by the GO film and air, as shown in Fig. 1(b). The GO ultrathin flat lens is able to modulate both phase and amplitude simultaneously from the conversion of GO to rGO. During the conversion[31,32], the GO film shows three continuously tunable physical property variations: the reduction of film thickness, the increase of refractive index and the decrease of transmission. These three property variations provide the required phase and amplitude modulation in designing a GO lens. The GO lenses can be one-step fabricated by the direct laser writing technology[33], which introduces localized rGO region by a tightly focused laser beam.

To design the GO lens with the targeted focal length f and diameter D based on the RS diffraction theory, we consider the intensity distribution on the z axis, namely

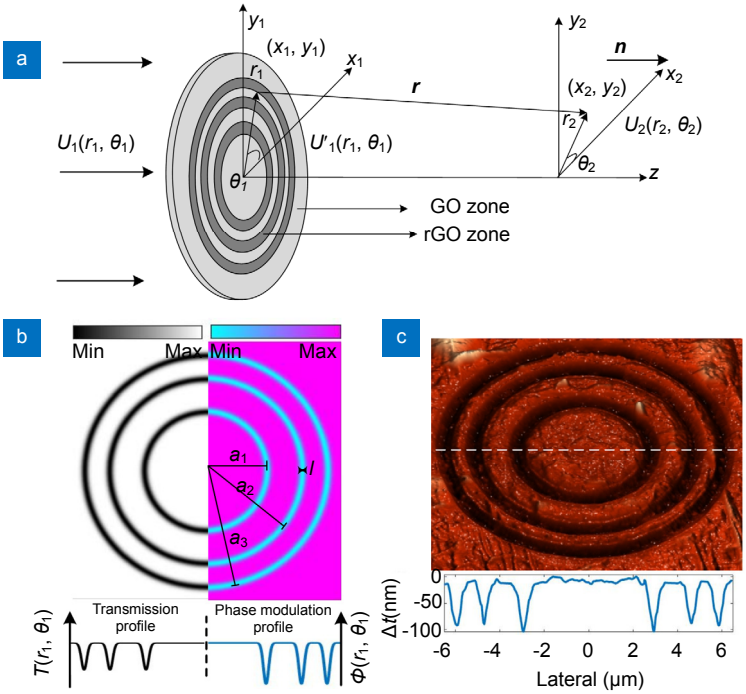

Fig. 1 | The design of the GO ultrathin flat lens. (**a**) Diffraction of GO ultrathin flat lens in polar and Cartesian coordinate systems. (**b**) Transmission and phase modulations provided by the GO lens. (**c**) Topographic profile of the GO ultrathin flat lens measured by an atomic force microscope.

r_2=0, z=f. And based on the Euler's equation, the expression of intensity distribution on the z axis can be simplified to (Supplementary Section 1):

$$I(r_1)=(\frac{2\pi f}{\lambda})^2(\omega^2+v^2), \quad (3)$$

here $$\omega=\int_0^{\infty}U_1(r_1)\frac{\cos(-k\sqrt{f^2+r_1^2})}{f^2+r_1^2}r_1dr_1 \ ,$$

$$v=\int_0^{\infty}U_1(r_1)\frac{\sin(-k\sqrt{f^2+r_1^2})}{f^2+r_1^2}r_1dr_1 \ .$$

The maximal destructive interference positions on the intensity distribution $I(r_1)$ predict the ring radii of the GO lens with a focal length f. In the meantime, the diameter is decided by the number of rings. In this way, the lenses can be designed according to different incident fields ($U_1(r_1,\theta_1)$).

On the other hand, for a situation that the observation point is not far away from the optical axis, it is assumed $|(r_1^2-r_2^2)/z^2|\ll 1$, which is the paraxial approximation, Eq. (1) can be reduced to the Fresnel diffraction as[28]:

$$U_2(r_2,z)=\frac{i2\pi}{\lambda z}\exp(-ikz)\exp(-\frac{ikr_2^2}{2z})$$
$$\cdot\int_0^{\infty}U_1'(r_1)\exp(-\frac{ikr_1^2}{2z})J_0(\frac{kr_1r_2}{z})r_1dr_1. \quad (4)$$

According to the Fresnel diffraction theory, the radii of a Fresnel zone plate can be defined as follows[18]:

$$r_m=\sqrt{m\lambda f+(\frac{m\lambda}{2})^2} \ , \quad (5)$$

where f is the focal length, r_m is the outer radius of the m^{th} zone.

Results and discussion

We first compare the lens designs using the RS and the Fresnel methods. The targeted focal length is 3.1 μm (Lens 1) with a lens thickness of 0.2 μm. The lenses are composed of three concentric rings with radii of a_1, a_2 and a_3. Here we assume the incident beam is a plane wave. The resulted plots of radii of the rings are shown in Fig. 2. There is a significant difference (0.215 μm or 13.9%) between the radii of the two models at the first ring, and the differences decrease to 0.175 μm (6.6%) for the second ring, and 0.157 μm (4.4%) for the third ring.

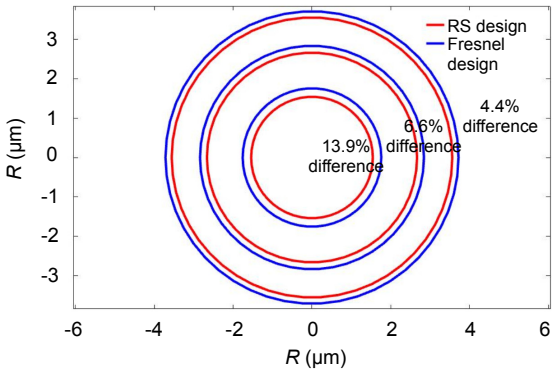

Fig. 2 | Comparison of radii of the two different theoretical flat lens designs.

To verify the two designs, we numerically simulate the intensity distributions based on the RS diffraction theory and compared to the Fresnel design. The results are

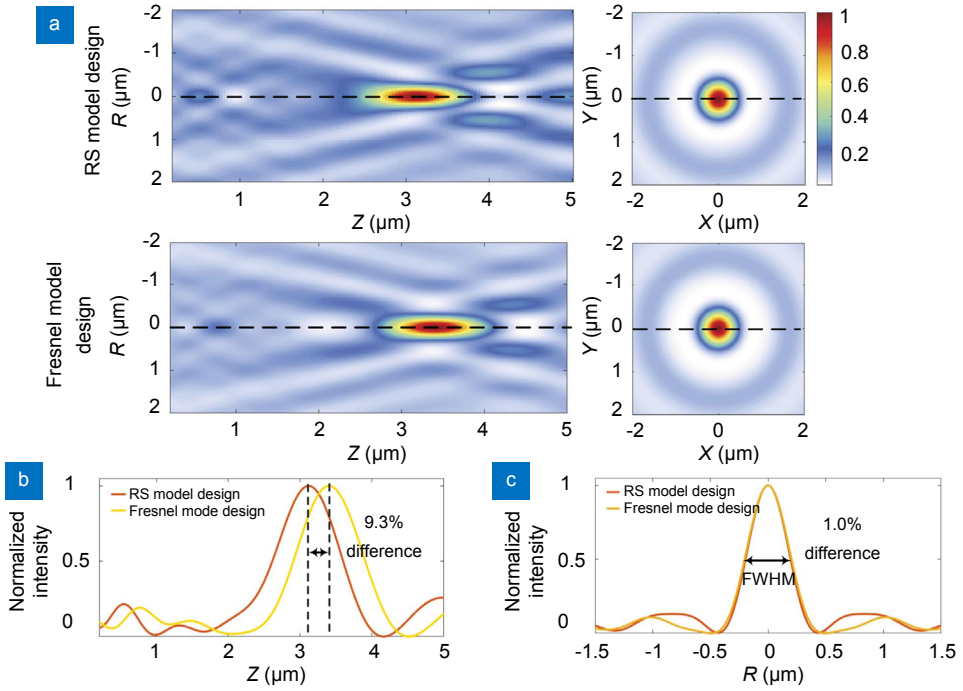

Fig. 3 | Intensity distribution of the two designs based on the RS diffraction theory. (**a**) Intensity distributions in the lateral and axial planes. (**b**) Cross-sectional intensity distribution along the black dash lines in the axial planes. (**c**) Cross-sectional intensity distribution along the black dash lines parallel to the *x* axis in the lateral planes.

shown in Fig. 3. The transverse full widths at a half maximum (FWHMs) of the focal spots are similar (1.0% difference, Fig. 3(c)) for the two designs. The effective NA of the GO lens can be calculated as $NA=0.61\lambda/FWHM$, which is 0.82. However, on the z axis (Fig. 3(b)), we can see clearly the difference (9.3%) of the focal lengths between the two designs. The RS model design provides a focal length of 3.11 μm as the design specified, whereas the Fresnel model design gives a 3.40 μm focal length which has a 9.3% deviation. Therefore, for high NA GO lenses, the RS method is able to design lenses according to the requirements with a high accuracy, in contrast to the Fresnel model.

In addition, to demonstrate the flexibility of the RS method, another lens (Lens 2) with 9.1 μm focal length is designed by the RS method. To verify the accuracy of the RS method, these two lenses are analyzed using the RS and Fresnel diffraction theories, and compared with the FDTD model and the experimental results. The parameters of the two lenses are shown in Table 1. The lenses are fabricated using direct laser writing with a femtosecond laser (Coherent®, Libra, λ=800 nm, pulse width is 100 fs, repetition rate is 10 kHz, the setup information can be found in Supplementary Section 2). We use Gaussian function to express the modulation of the complex refractive index and the depth profiles (Fig. 1(b)), which is confirmed by the atomic force microscope (AFM) measurement of the fabricated lens (Fig. 1(c)). The thickness of the GO region is ~200 nm, and the thickness of the thinnest rGO region is ~100 nm, as shown in the topographic profile of Lens 2 in Fig. 1(c). The FWHM of the Gaussian profiled lines is ~300 nm.

Table 1 | Radii of Lens1 and Lens2

	Lens 1 (μm)	Lens 2 (μm)
a_1	1.543	3.135
a_2	2.665	4.670
a_3	3.559	5.903

The focal intensity distributions of the lenses are measured using a microscopic imaging setup (Supplementary Section 3). The experimentally measured focal intensity distributions of Lens 1 in the x-y and x-z planes and the corresponding theoretical results from the FDTD, RS and Fresnel theoretical calculations are shown in Fig. 4(a).

To see the effect of the incident polarizations, we assume the incident light polarizing along the x-direction in the FDTD simulation. The intensity distributions along the directions parallel (x-direction) and vertical (y-direction) to the polarization of the incident beam are shown in Fig. 4(c) with dash lines. The FWHM of the focal spot along the x and y directions of the FDTD results are ~0.50 μm (0.79 λ) and ~0.46 μm (0.73 λ), respectively (Table 2). The FWHM of the focal spot predicted by the RS diffraction theory is ~0.47 μm (0.74 λ) (Table 2). No remarkable difference (< 6% in the x direction and 2.1% in the y direction) can be found between the FDTD and RS theoretical results, which is expected considering the effective NA of the lens is approximately 0.82. Based

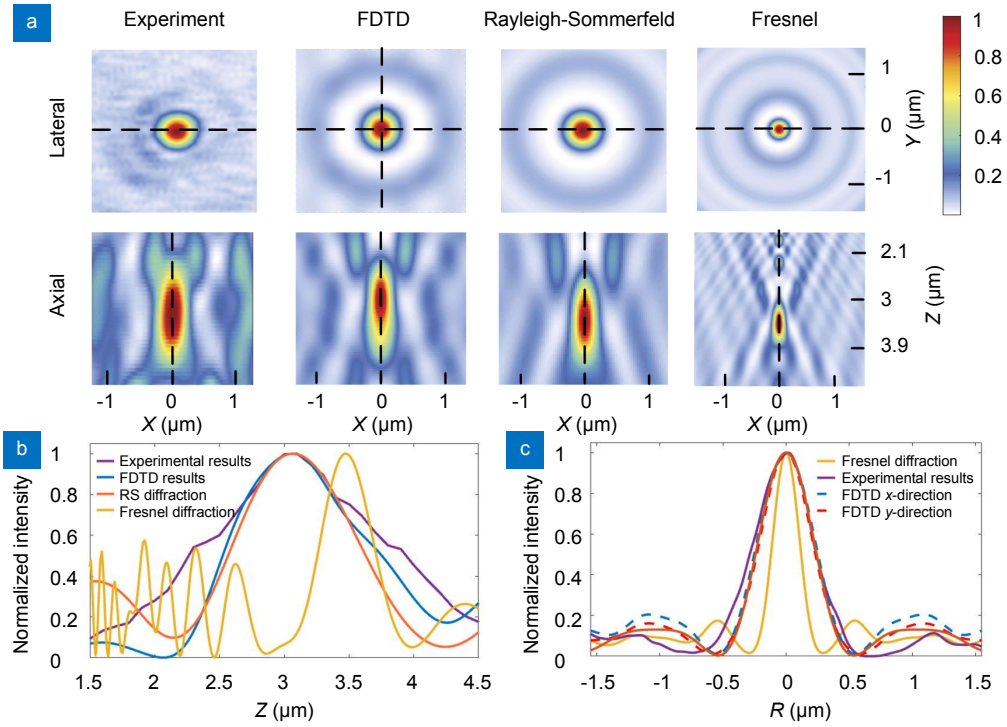

Fig. 4 | Intensity distributions of theoretical and experimental results of Lens 1. (**a**) Intensity distributions in the lateral and axial planes. (**b**) Intensity distribution along the black dash lines in the axial planes. (**c**) Intensity distribution along the black dash lines parallel to the x axis in the lateral planes.

on this result, we can conclude that the scalar RS diffraction theory is able to predict the focusing intensity distributions of the GO lenses accurately.

One can see that the match between the FDTD simulation, RS theoretical calculation and the experimental results are reasonably good. In comparison, significant difference can be identified in the Fresnel theoretical results, which gives a much smaller focal spot both in the *x*-*y* and *x*-*z* planes. For further detailed comparisons, the intensity distribution along the *x* and *z* directions (marked by the black dash lines) of all results are plotted in the same figures (Figs. 4(b) and 4(c)). The designed focal length of Lens 1 is 3.1 μm. The resulted focal lengths of the experimental measurement, the FDTD simulation, the RS theoretical results are 3.09 μm, 3.07 μm and 3.11 μm, respectively (Table 2). However, the Fresnel theoretical result is 3.48 μm. In addition, the experimental result of the FWHM is 0.51 μm (0.81 λ), which is only 2% difference from the FDTD result (*x*-direction) and 7.8% difference from the RS theoretical calculation. In comparison, the FWHM prediction using the Fresnel diffraction model is only 0.24 μm (0.38 λ), which shows 52.1% and 52.9% differences compared with the FDTD model and experimental result, respectively. It shows that, the RS diffraction theory can predict the focusing process accurately for a high *NA* lens, in contrast to the Fresnel diffraction theory, which shows non-negligible difference.

For the Lens 2 case, the focal length and diameter of the lens are 2–3 times of those used in Lens 1, the FDTD requires nearly 20 times of simulation resources and time. Under such a circumstance, only the results from experiment, RS and Fresnel theoretical calculations are shown in Fig. 5. The cross-sectional intensity plots along the axial and lateral directions are shown in Figs. 5(b) and 5(c), respectively. It is noticed that the experimental results and the simulations using the RS diffraction theory match well, while the focal length calculated by the Fresnel diffraction theory is significantly different from the others.

Table 2 | Focal lengths *f* and FWHMs of the theoretical and experimental results of Lens 1 and Lens 2

	Lens 1		Lens 2	
	f (μm)	FWHM (μm)	*f* (μm)	FWHM (μm)
RS theory	3.11	0.47	9.14	0.54
FDTD (*x*-direction)	3.07	0.50	-	-
FDTD (*y*-direction)	3.07	0.46	-	-
Fresnel theory	3.48	0.24	10.28	0.50
Experiment	3.09	0.51	9.15	0.56

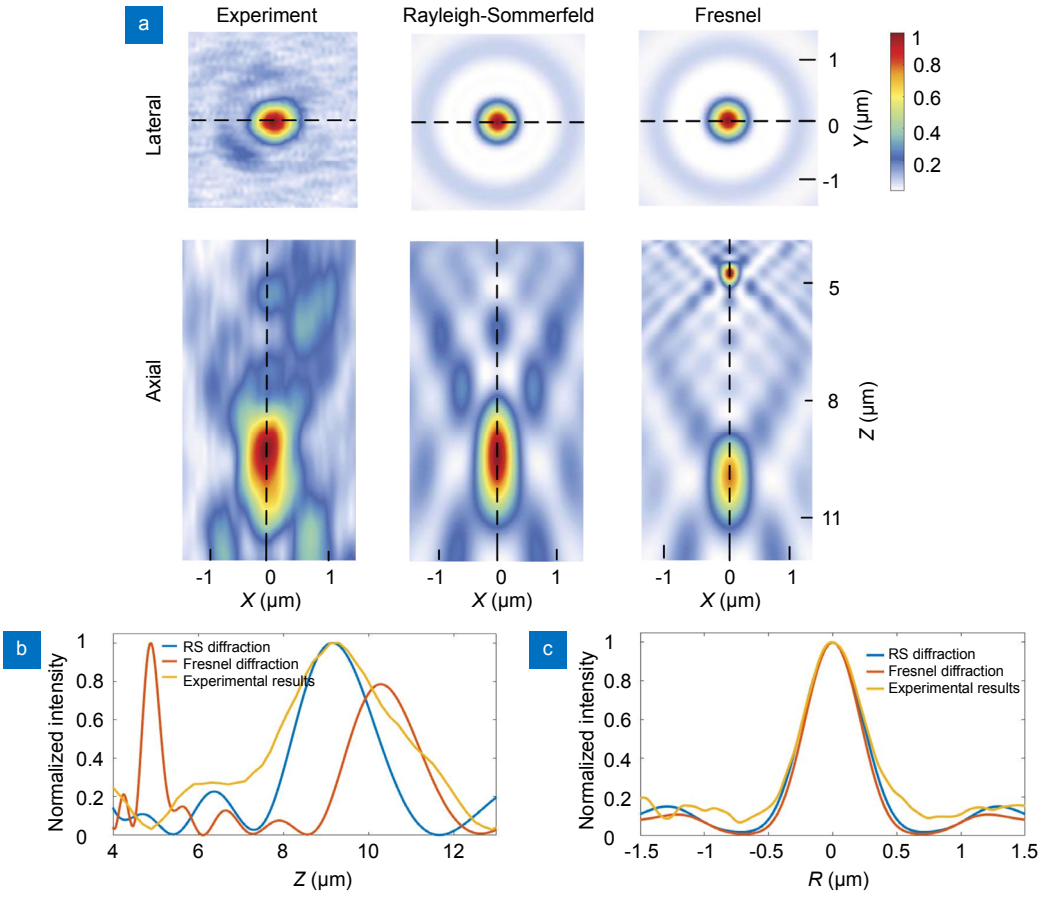

Fig. 5 | Intensity distributions of theoretical and experimental results of Lens 2. (**a**) Intensity distributions in the lateral and axial planes. (**b**) Intensity distributions along the black dash lines in the axial planes. (**c**) Intensity distributions along the black dash lines in the lateral planes.

The FWHMs and focal lengths are listed in Table 2. The FWHMs of the experimental result, the RS and the Fresnel theoretical calculations are 0.56 μm (0.89λ), 0.54 μm (0.86λ) and 0.50 μm (0.79λ), respectively. The difference between the experimental result and RS theoretical calculation is 3.7%, confirming the high accuracy of the RS diffraction theory as expected. Meanwhile, the difference between the experimental result and the Fresnel theoretical result is 11.4%. Although the difference for the Fresnel result is still larger than the RS result, it is much smaller compared with the previous case because the effective NA of Lens 2 is smaller (0.71). Whereas, the focal length calculated by the Fresnel theory (10.28 μm) is much larger than the experimental results (9.14 μm) and that from the RS theory (9.15 μm). In addition, there is a false focal spot at around 5 μm in the Fresnel diffraction model, which is not observed in the experimental result. Therefore, under such a circumstance, the Fresnel diffraction theory still fails to give an accurate description of the performance of the GO lens.

Conclusion

In conclusion, we have developed a design method based on the RS diffraction theory, which is able to accurately design GO lenses with arbitrary focal length and diameter without the optimization process for the first time. Compared with the Fresnel model design, it is only applicable for low NA lenses satisfying the paraxial condition. The differences in the ring positions and the resulted focal length are approximately 13.9% and 9.1%, respectively, for the high NA GO lens we targeted. Furthermore, the design flexibility of the RS method has been demonstrated by two GO lenses with desired focal lengths and NAs. The accuracy of our design methods has been verified both experimentally through laser assisted fabrication and point spread function characterized as well as the FDTD simulation. The theoretical and experimental results show that the RS diffraction theory is able to accurately calculate the focusing process of GO lenses with arbitrary NA and focal lengths with a high speed and efficiency. Therefore, the demonstrated RS method is expected to find broad applications in designing and analyzing other ultrathin flat lenses, including metasurface lenses and lenses made of other 2D materials.

References

1. Mahajan V N. *Aberration Theory Made Simple* (SPIE Optical Engineering Press, Bellingham, WA, 1991).
2. Lu D, Lin Z W. Hyperlenses and metalenses for far-field super-resolution imaging. *Nat Commun* **3**, 1205 (2012).
3. Liu Z W, Steele J M, Srituravanich W, Pikus Y, Sun C *et al*. Focusing surface plasmons with a plasmonic lens. *Nano Lett* **5**, 1726–1729 (2005).
4. Fang N, Lee H, Sun C, Zhang X. Sub-diffraction-limited optical imaging with a silver superlens. *Science* **308**, 534–537 (2005).
5. Verslegers L, Catrysse P B, Yu Z, White J S, Barnard E S *et al*. Planar lenses based on nanoscale slit arrays in a metallic film. *Nano Lett* **9**, 235–238 (2009).
6. Yu N F, Capasso F. Flat optics with designer metasurfaces. *Nat Mater* **13**, 139–150 (2014).
7. Kildishev A V, Boltasseva A, Shalaev V M. Planar photonics with metasurfaces. *Science* **339**, 1232009 (2013).
8. Aieta F, Genevet P, Kats M A, Yu N F, Blanchard R *et al*. Aberration-free ultrathin flat lenses and axicons at telecom wavelengths based on plasmonic metasurfaces. *Nano Lett* **12**, 4932–4936 (2012).
9. Rogers E T F, Lindberg J, Roy T, Savo S, Chad J E *et al*. A super-oscillatory lens optical microscope for subwavelength imaging. *Nat Mater* **11**, 432–435 (2012).
10. Qin F, Huang K, Wu J F, Teng J H, Qiu C W *et al*. A supercritical lens optical label-free microscopy: Sub-diffraction resolution and ultra-long working distance. *Adv Mater* **29**, 1602721 (2017).
11. Zheng X R, Jia B H, Lin H, Qiu L, Li D *et al*. Highly efficient and ultra-broadband graphene oxide ultrathin lenses with three-dimensional subwavelength focusing. *Nat Commun* **6**, 8433 (2015).
12. Gao H W, Hyun J K, Lee M H, Yang J C, Lauhon L J *et al*. Broadband plasmonic microlenses based on patches of nanoholes. *Nano Lett* **10**, 4111–4116 (2010).
13. Wang Y X, Yun W B, Jacobsen C. Achromatic Fresnel optics for wideband extreme-ultraviolet and X-ray imaging. *Nature* **424**, 50–53 (2003).
14. Wang S C, Ouyang X Y, Feng Z W, Gao Y Y, Gu M *et al*. Diffractive photonic applications mediated by laser reduced graphene oxides. *Opto-Electron Adv* **1**, 170002 (2018).
15. Zheng X R, Lin H, Yang T S, Jia B H. Laser trimming of graphene oxide for functional photonic applications. *J Phys D: Appl Phys* **50**, 074003 (2017).
16. Ojeda-Castañeda J, Gómez-Reino C. *Selected Papers on Zone Plates* (SPIE Press, Bellingham, WA, 1996).
17. Cao Q, Jahns J. Modified Fresnel zone plates that produce sharp Gaussian focal spots. *J Opt Soc Am A* **20**, 1576–1581 (2003).
18. Yu Y H, Tian Z N, Jiang T, Niu L G, Gao B R. Fabrication of large-scale multilevel phase-type Fresnel zone plate arrays by femtosecond laser direct writing. *Opt Commun* **362**, 69–72 (2016).
19. Wang X K, Xie Z W, Sun W F, Feng S F, Cui Y *et al*. Focusing and imaging of a virtual all-optical tunable terahertz Fresnel zone plate. *Opt Lett* **38**, 4731–4734 (2013).
20. Saavedra G, Furlan W D, Monsoriu J A. Fractal zone plates. *Opt Lett* **28**, 971–973 (2003).
21. Solak H H, David C, Gobrecht J. Fabrication of high-resolution zone plates with wideband extreme-ultraviolet holography. *Appl Phys Lett* **85**, 2700–2702 (2004).
22. Kunz K S, Luebbers R J. *The Finite Difference Time Domain Method for Electromagnetics* (CRC Press, Roca Raton, FL, 1993).
23. Taflove A. Review of the formulation and applications of the finite-difference time-domain method for numerical modeling of electromagnetic wave interactions with arbitrary structures. *Wave Motion* **10**, 547–582 (1988).
24. Zhang H R, Zhang F C, Liang Y, Huang X G, Jia B H. Diodelike asymmetric transmission in hybrid plasmonic waveguides via breaking polarization symmetry. *J Phys D: Appl Phys* **50**, 165104 (2017).
25. Byrnes S J, Lenef A, Aieta F, Capasso F. Designing large, high-efficiency, high-numerical-aperture, transmissive meta-lenses for visible light. *Opt Express* **24**, 5110–5124 (2016).

26. Zhuang Z F, Yu F H. Optimization design of hybrid Fresnel-based concentrator for generating uniformity irradiance with the broad solar spectrum. *Opt Laser Technol* **60**, 27–33 (2014).
27. Huang K, Shi P, Kang X L, Zhang X B, Li Y P. Design of DOE for generating a needle of a strong longitudinally polarized field. *Opt Lett* **35**, 965–967(2010).
28. Gu M. *Advanced Optical Imaging Theory* (Springer, Berlin Heidelberg, 2000).
29. Goodman J W. *Introduction to Fourier Optics* (McGraw-Hill, New York, 1968).
30. Hecht E. *Optics* 4th ed (Addison-Wesley, Boston, 2002).
31. Zheng X R, Jia B H, Chen X, Gu M. In situ third-order non-linear responses during laser reduction of graphene oxide thin films towards on-chip non-linear photonic devices. *Adv Mater* **26**, 2699–2703 (2014).
32. Li X P, Zhang Q M, Chen X, Gu M. Giant refractive-index modulation by two-photon reduction of fluorescent graphene oxides for multimode optical recording. *Sci Rep* **3**, 2819 (2013).
33. Yang T S, Lin H, Jia B H. Two-dimensional material functional devices enabled by direct laser fabrication. *Front Optoelectron* **11**, 2–22 (2018).

Acknowledgements

B H Jia acknowledges the support from Australian Research Council and Defence Institute Australia.

Competing interests

The authors declare no competing financial interests.

Supplementary information

Supplementary information is available for this paper at https://doi.org/10.29026/oea.2018.180012

Section 1: Lens design method
Section 2: Experimental setup of the laser fabrication system (Fig. S1)
Section 3: Experimental setup of the GO lens characterization (Fig. S2)